Journal Name

ARTICLE

Photoelectron spectroscopic study of $I^-{\cdot}ICF_3$: A frontside attack S_N2 pre-reaction complex

Received 00th January 20xx,
Accepted 00th January 20xx

DOI: 10.1039/x0xx00000x

www.rsc.org/

Golda Mensa-Bonsu,[a] David J. Tozer[a] and Jan R. R. Verlet[†a]

Photodetachment and 2D photoelectron spectra of the mass-selected $I^-{\cdot}CF_3I$ complex are presented together with electronic structure calculations. Calculations show that the I^- is located at the iodine side of CF_3I. Vertical and adiabatic detachment energies were measured at 4.03 and approximately 3.8 eV, respectively. The photoelectron spectra and molecular orbitals show a significant covalent bonding character in the cluster. The presence of electronic excited states is observed. Below threshold, iodide is generated which can be assigned to the photoexcitation of degenerate charge-transfer bands from the off-axis p-orbitals localised on iodide. Near the onset of two spin-orbit thresholds, bright excited states are seen in the experiment and calculations. Excitation of these leads to the formation of slow electrons. The spectroscopy of $I^-{\cdot}CF_3I$ is compared to the well-studied $I^-{\cdot}CH_3I$ cluster, a pre-reaction complex in the text-book $I^- + CH_3I$ S_N2 reaction. Despite the reversed stereodynamics (*i.e.* inversion of the CX_3 between X = H and F) of the S_N2 reaction, striking similarities are seen. Both complexes possess charge transfer excited states near their respective vertical detachment energies and exhibit vibrational structure in their photoelectron spectra. The strong binding is consistent with observations in crossed molecular beam studies and molecular dynamics simulations that suggest that iodine as a leaving group in an S_N2 reaction affects the reaction dynamics.

Introduction

Bimolecular nucleophilic substitution (S_N2) reactions represent a cornerstone of reactivity in organic chemistry.[1] In its simplest form, the reaction $X^- + CH_3Y \rightarrow XCH_3 + Y^-$ involves the text-book $[X\cdots CH_3\cdots Y]^-$ activated complex, where X^- attacks CH_3Y from the backside. The stereodynamics of the reaction are expected from the long-range charge-dipole moment interaction between X^- and CH_3Y. While in the solution phase, this long-range interaction is screened, the isolated view of the reaction remains mostly valid.[2–4] As a result, there have been many studies of S_N2 reaction dynamics in the gas-phase, which have provided exquisite insight into the reaction mechanisms over many years.[5–8] While the indirect, backside attack mechanism has been researched in-depth, contemporary experimental and computational studies have explored alternative mechanistic pathways of the S_N2 reaction.[9–12] For example, recent crossed molecular beam studies and atomistic molecular dynamics simulations have shown how the dynamics of the reaction are sensitive to the leaving group, with differing mechanisms contributing when Y is changed.[9] Additionally, photoelectron (PE) spectroscopy of the pre-reaction complex, $X^-\cdots CH_3Y$, can provide much insight about the entrance channel of the reaction, which often plays a deterministic role in the reaction.[13,14] However, in PE spectroscopy experiments, it has not been possible to control the stereodynamics of the pre-reaction complex and, hence, only the backside attack (direct rebound) mechanism has been probed. In the present study, we make a chemical substitution of the methyl H-atoms to F-atoms. As the H atoms are mostly indirectly involved in the S_N2 reaction, the main reaction coordinate along the X–C–Y bond is preserved.[1] However, this chemical substitution reverses the stereodynamics of the reactions and allows us to perform PE spectroscopy of the pre-reaction complex for the frontside attack (along the X–Y–C coordinate).

The gas-phase S_N2 reaction has been studied extensively by the groups of Wester and Hase;[8,10,15–17] they have recently observed that the replacement of the leaving group Y from Cl to I in the S_N2 reaction, $F^- + CH_3Y$, has dramatic effects on the reaction dynamics.[9] Specifically, for Y = Cl, the dominant reaction mechanism is the classic direct rebound mechanism (at energies > 0.6 eV).[9,18–20] In contrast, a significant fraction of reactions for the Y = I reaction could be attributed to a direct stripping mechanism, especially at high impact parameters, where the F^- attacks the CH_3 and leads to the product ion leaving along the initial direction of the CH_3Y reactant.[9] Given that the permanent dipole moments of CH_3Cl and CH_3I are not that different (μ = 1.90 D and μ = 1.64 D, respectively[21]), the change in dynamical orientation of CH_3I was assigned to a stronger interaction between the two halogen atoms in the Y = I reaction (the $F^-\cdots ICH_3$ complex is bound by 0.97 eV, while $F^-\cdots ClCH_3$ is bound by only 0.14 eV).[9] This stronger interaction

[a] Department of Chemistry, Durham University, Durham DH1 3LE, United Kingdom.
† E-mail: j.r.r.verlet@durham.ac.uk

changes the orientation at short range leading to differing reaction dynamics.

The most studied pre-reaction S_N2 complex using PE spectroscopy has been $I^-\cdots CH_3I$.[13,22–30] Cyr *et al*. employed PE, photodetachment and photofragment spectroscopy to characterise the electronic excited states of $I^-\cdots CH_3I$, which provided evidence of an intra-cluster charge transfer state with I^- and CH_3I as the respective donor and acceptor species.[22,23,25] Although their studies did not indicate that the S_N2 reaction could be photoinitiated, the knowledge gained of the $I^-\cdots CH_3I$ complex establishes this system as an ideal test-case to make the H to F substitution and to provide insight into the above-mentioned molecular beam and molecular dynamics simulation studies. We show that, despite the reversed stereochemistry, similarly strong photoabsorption at threshold is observed for $I^-\cdots CH_3I$ and $I^-\cdots ICF_3$ and many of the spectral features are common to both systems.

It is also noteworthy that $I^-\cdots ICF_3$ is potentially an important species in plasma chemistry. Industrially, plasma etching is widely used to fabricate the fine structural components of microelectronic devices.[31,32] While cations are primarily considered in plasmas, anions are also present and contribute to the chemical cocktail.[33] The most common process gases for plasma etching include CF_4 and CF_3H.[32,34] However, these are long-lived global warming gases necessitating their reduced usage.[35] Alternatives such as CF_3I, which has a relatively low global-warming potential,[36–39] have been shown to have similar etching rates to standard mixtures.[36,40] However, much less is known about the composition of these plasmas.[41] Dissociative electron attachment to CF_3I forms I^- in high yield,[42] which may go on to complex to the abundant CF_3I process gas to form species such as $I^-\cdots ICF_3$. Hence, these species may be common chemical species in the plasma mix, but have yet to be studied. The present work shows that $I^-\cdots ICF_3$ has a large electron affinity and is strongly bound suggesting that such species may indeed play a role in plasma chemistry.

Experimental & Computational Details

A detailed description of the experimental setup will be presented elsewhere and only a brief overview is given here. To generate $I^-\cdots ICF_3$, a CF_3I/Ar mix was expanded through a pulsed Even-Lavie valve into vacuum.[43] The molecular beam expansion was intersected by an electron beam (300 eV) near the throat of the expansion, generating an electron rich plasma in the high molecular density region. The subsequent expansion and associated cooling provides a snap-shot of the species formed in the plasma.[44] Anions are extracted from the molecular beam using a linear Wiley-Mclaren time of flight spectrometer.[45] This showed that the dominant species formed were I^- (which is to be expected from the dissociative electron attachment to CF_3I) together with $I^-\cdots ICF_3$, formed presumably by the condensation of a CF_3I onto I^- because of the long-range charge-dipole interaction. We also observed larger clusters with chemical formula $I^-(CF_3I)_n$. The mass-selected $I^-\cdots ICF_3$ was crossed by nanosecond laser pulses from a Nd:YAG (3rd harmonic) pumped optical parametric oscillator at the focus of the mass-spectrometer. The ejected PEs were accelerated perpendicular to the ion and laser beam axes towards a position-sensitive detector in a velocity-map imaging spectrometer.[46,47] The focus of the mass-spectrometer was tuned to coincide with the laser/ion interaction point. The PE spectra were reconstructed from the raw images using the polar onion-peeling algorithm.[48] The electron kinetic energy (eKE) scale was calibrated to the known PE spectrum of I^-. The PE spectrometer had a resolution of $\Delta eKE/eKE < 3\%$.

Density functional theory (DFT)[49] and time-dependent DFT (TDDFT)[50] calculations were performed to provide a qualitative interpretation of the experimental results and a basic understanding of the electronic structure of $I^-\cdots ICF_3$. For comparative purposes, calculations were also performed on $I^-\cdots CH_3I$. It is well known that many approximate exchange-correlation functionals suffer from formal problems for anions (namely positive highest occupied molecular orbital energies), but this can be unproblematic in practical calculations.[51–56] In the present study, all reported theoretical results were determined using the CAM-B3LYP range-separated exchange-correlation functional,[57] for which these formal problems are largely overcome.[58] This functional also contains the relevant physics for describing long-range and charge-transfer excitations, which are relevant to the systems considered.[59] A further difficulty with describing excited states of anions is that many may be resonances, meaning they must be distinguished from discretized continuum states. We used a standard, basis function exponent-scaling stabilisation approach[60] to ensure that the excited states reported are appropriate.

The 6-311++G** basis set was used on C, F, and H atoms,[61–63] while LANL2DZdp was employed in calculations for the I atoms.[64–66] The calculated ground state optimised geometries were verified to be minima by vibrational analysis and TDDFT calculations were performed at the optimised geometries. We note that our calculations do not include spin-orbit interactions. For iodine, this is of course a major omission – the iodine spin-orbit splitting in the two ^2P_J states of iodine is 0.94 eV – and this is not quantitatively reflected in the present calculations. Nevertheless, the calculations provide a useful qualitative basis to assist the interpretation of the experimental results. The Gaussian G09 package has been used throughout.[67]

Results

To determine the ground state geometries, optimisations were performed commencing from frontside and backside (regular S_N2) conformations. The lowest energy structure of $I^-\cdots ICF_3$ has C_{3v} symmetry, with I–I and I–C bond lengths of 3.33 and 2.18 Å, respectively (see Figure 1). In contrast to $I^-\cdots CH_3I$, the perfluorinated $I^-\cdots ICF_3$ has the I^- residing on the side of the iodine, *i.e.* frontside attack. We have verified that this frontside structure is also obtained when a D3 dispersion[68] correction is introduced or when MP2 is used.[69] The change in orientation of CX_3I between X = H and F correlates with the reversal in permanent dipole moment between CH_3I and CF_3I.

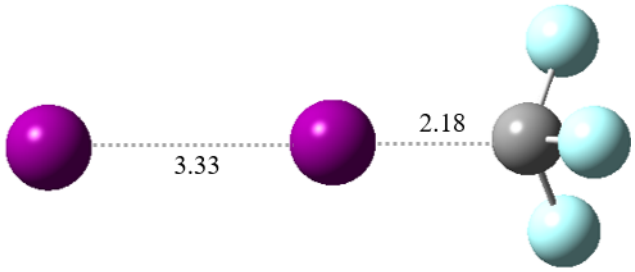

Figure 1: Calculated ground state structure of $I^-\cdots ICF_3$. Bond distances are shown in Angstroms.

The electropositive H atoms lead to a dipole moment μ = 1.78 D in the direction of the I–C bond,[70] while the strongly electronegative F atoms lead to a dipole moment μ = 1.28 D in the antiparallel direction.[71] The dipole moment vector reversal has the interesting consequence that one can still view $I^-\cdots ICF_3$ as a reaction precomplex, but with different stereochemistry, and hence, the spectroscopic signatures may be expected to be different between X = H and F.

Figure 2 shows the frequency-resolved (2D) PE spectra collected over the 3.50 ≤ *hv* ≤ 5.50 eV range with 0.1 eV intervals. 2D PE spectroscopy is a powerful probe of the location and dynamics of anionic resonances,[72] which we have recently applied to radical anions,[73,74] biomolecules [75] and clusters.[76–79] Individual PE spectra are plotted in terms of electron binding energy eBE = *hv* – eKE and have been normalised to their maximum intensity. At *hv* = 3.50 eV, a narrow peak is visible at eBE = 3.06 eV. The profile and position of this peak indicates that it arises from direct photodetachment from atomic I^- to the neutral iodine $^2P_{3/2}$ ground state. This peak can be clearly identified in the 3.5 ≤ *hv* ≤ 3.9 eV range, although it is also present at higher photon energies (with much reduced intensity). The appearance of the I^- PE spectrum following the excitation of $I^-\cdots ICF_3$ implies that two sequential photons were absorbed during the laser pulse (~5 ns).

At *hv* ≥ 5.2 eV, two broad direct detachment features dominate the PE spectrum. The peaks centred around eBE = 4.0 and 4.9 eV have similar spectral shapes and widths. The energy gap between the two features is ~0.9 eV, which is close to the spin-orbit splitting in the neutral iodine atom (0.94 eV). We assign these two peaks to the direct detachment from $I^-\cdots ICF_3$, leaving the neutral as $I[^2P_{1/2}]\cdots ICF_3$ and $I[^2P_{3/2}]\cdots ICF_3$ for the high and low eBE peaks, respectively. The vertical detachment energy (VDE) of $I^-\cdots ICF_3$ corresponds to the maximum of the $[^2P_{3/2}]\cdots ICF_3$ peak; VDE = 4.03±0.05 eV (calculated at 4.29 eV). The large spectral width of the peaks (~0.3 eV) and their unresolved vibrational structure could preclude the observation of the 0-0 transition and, thus, also the direct measurement of the adiabatic detachment energy, ADE. Nevertheless, taking the lowest eBE where PE signal becomes apparent from the direct detachment provides a measure of ADE = 3.8±0.1 eV. This is a blue-shift of >0.7 eV compared to unclustered I^-, and much larger than the blue-shift observed in $I^-\cdots CH_3I$ (0.38 eV).[25]

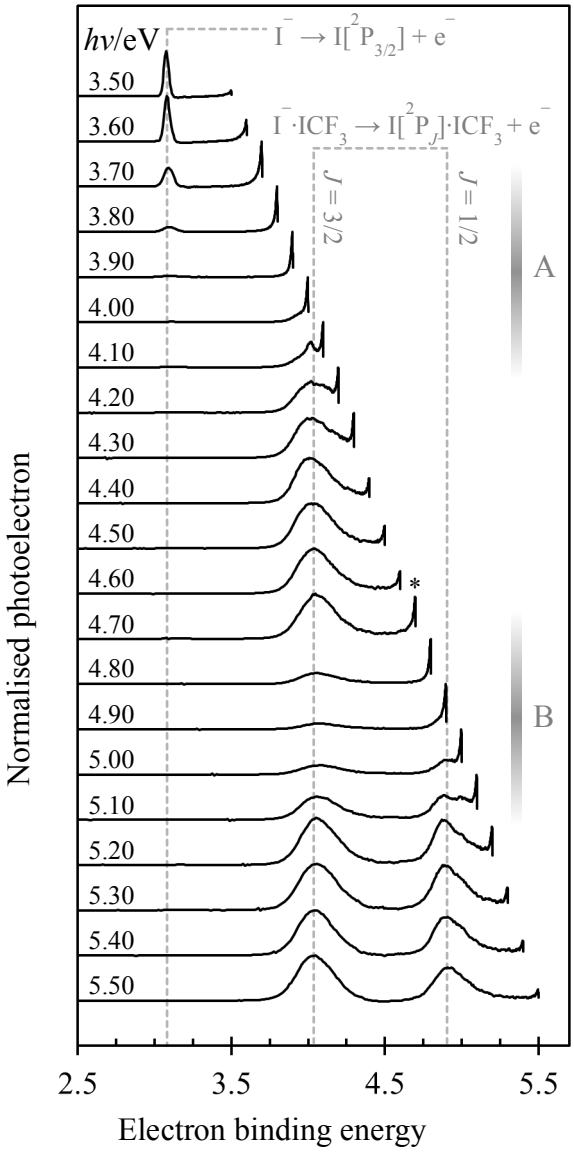

Figure 2: 2D photoelectron spectra of $I^-\cdots ICF_3$ in the 3.50 ≤ *hv* ≤ 5.50 eV range with *hv* indicated on the left of each offset spectrum. The spectra have been normalised to their maximum intensity. Bands are labelled according to their detachment process (see text for details). Bands A and B indicate regions where indirect processes dominate, which are evident from the peak at near zero kinetic energy, which has, for example, been marked with an asterisk in the spectrum at *hv* = 4.70 eV.

The PE spectra corresponding to the direct detachment from $I^-\cdots ICF_3$ are on the whole unstructured. However, there is evidence of vibrational structure around *hv* ~ 4.1 and 5.1 eV. The *hv* = 5.10 eV PE spectrum, reproduced in Figure 3, shows two unresolved peaks superimposed on the broader background peak. The spacing between these two peaks is approximately 100 meV (800 cm^{-1}).

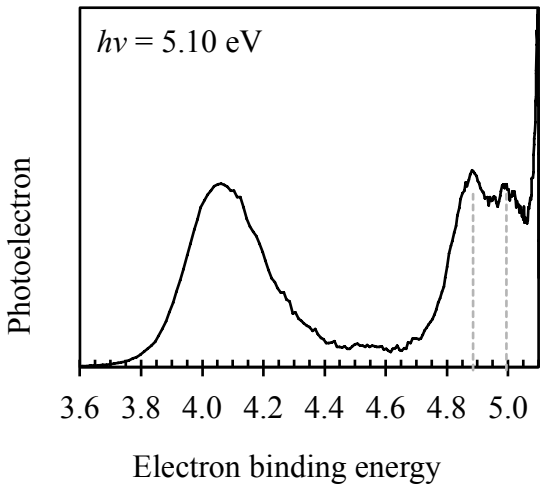

Figure 3. Photoelectron spectrum of $I^-\cdots ICF_3$ taken at *hv* = 5.10 eV. The vertical dashed lines indicate the vibrational structure observed.

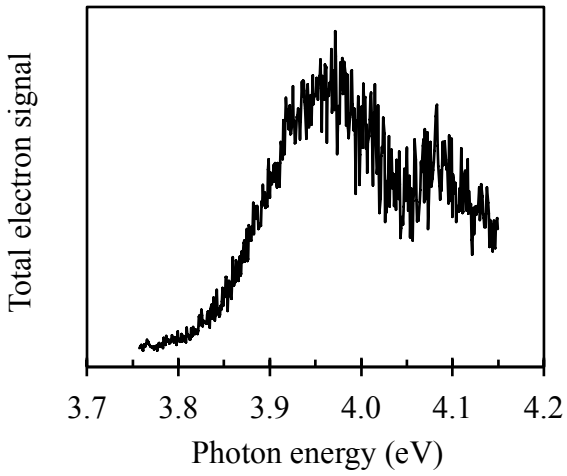

Figure 4: Photodetachment spectrum of $I^-\cdots ICF_3$ taken around the onset of the direct detachment from the cluster.

Additionally, present in virtually all PE spectra is a narrow detachment feature peaking at eBE = *hv*. As an example, this peak is labelled with an asterisk in the *hv* = 4.70 eV PE spectrum in Figure 2; it is also clearly visible in Figure 3. The peak corresponds to the production of PEs with near zero kinetic energy, which is normally associated with an indirect detachment process. Through comparison of the relative intensities of bands present in the PE spectra, the dominant electron loss processes can be identified at each photon energy. With reference to Figure 2, regions labelled as A and B contain PE spectra in which the indirect detachment is the dominant electron loss process occurring. Specifically, at *hv* ~ 4.0 eV and 4.9 eV, the fraction of electrons produced via the direct detachment channels appears at a minimum.

Region A (and B) led to a noticeable increase in total electron signal as a function of *hv*. To explore this further, in Figure 4, a photodetachment (total electron yield) spectrum is presented in the 3.75 ≤ *hv* ≤ 4.15 eV range. Two main peaks can be identified: a broad feature centred at *hv* = 3.97 eV, and a second, less prominent feature centred at *hv* = 4.07 eV. These peaks appear very close to the VDE of the cluster at 4.03 eV (and above the measured ADE = 3.8 eV). For a direct detachment process, a rise in the PE yield is expected when the photon energy passes through threshold, but this is expected to resemble a smooth step function.[80] Here, the observations of peaks in the photodetachment spectrum and the appearance of an indirect process for electron loss (Figure 2, spectral regions A and B), point to a photoexcitation of excited states of the cluster close to the detachment threshold.[80] A similar situation appears to be present at the onset of the second detachment threshold corresponding to the $I[^2P_{1/2}]\cdots ICF_3 + e^-$ channel.

Similar to the dominant indirect detachment processes occurring in regions A and B in the 2D PE spectra (Figure 2), the two-photon detachment process at eBE = 3.06 eV is mediated by an electronic excited state. To probe the character of the excited states, DFT and TDDFT calculations were performed.

The relevant molecular orbitals (MOs) of $I^-\cdots ICF_3$ are shown in Figure 5. The highest occupied MO (HOMO) corresponds primarily to the non-bonding atomic p-orbital localised on I and is doubly-degenerate (*i.e.* the p_x and p_y orbitals – only one of these is shown in Figure 5). The next lowest occupied MO, HOMO−2 corresponds to the p_z orbital on I which interacts with CF_3I. As a comparison, the analogous MOs for $I^-\cdots CH_3I$ are also included in Figure 5. The overall MO structure of $I^-\cdots CH_3I$ is very similar to that of $I^-\cdots ICF_3$, despite the reversed stereochemistry. However, it is also clear from the occupied MOs that the charge in $I^-\cdots ICF_3$ is more delocalised onto the CF_3I moiety and that $I^-\cdots ICF_3$ has more covalent bonding character than in $I^-\cdots CH_3I$, where the charge is mostly localised on the I atom. The lowest unoccupied MO (LUMO) in $I^-\cdots ICF_3$ and $I^-\cdots CH_3I$ are also shown in Figure 5.

Electronic excitation energies and their character were computed using TDDFT and the dominant orbital transitions are included in Figure 5. For $I^-\cdots ICF_3$, the lowest energy transitions were calculated at 4.04 eV and correspond to the HOMO/HOMO−1 → LUMO. These transitions have a low oscillator strength (0.009). Additionally, a very bright transition corresponding to the transition from HOMO−2 → LUMO, with an oscillator strength of 0.91, was identified in the relevant energy range. This bright state has been calculated at 4.82 eV above the anion ground state.

The excited states of $I^-\cdots CH_3I$ bear close similarities to those of $I^-\cdots ICF_3$. The lowest energy transitions of $I^-\cdots CH_3I$ also corresponds to the degenerate HOMO/HOMO−1 → LUMO excitation. This transition has a similarly low oscillator strength but is red-shifted by 0.27 eV compared to the analogous transition in $I^-\cdots ICF_3$. The analogous HOMO−2 → LUMO bright electronic transition is calculated to lie at 3.88 eV (c.f. 4.82 eV for $I^-\cdots ICF_3$) and has an oscillator strength of 0.33.

Discussion

The experimental VDE of $I^-\cdots ICF_3$ is 4.03 eV, which can be compared to that of the related $I^-\cdots CH_3I$ at 3.42 eV,[23,28] while

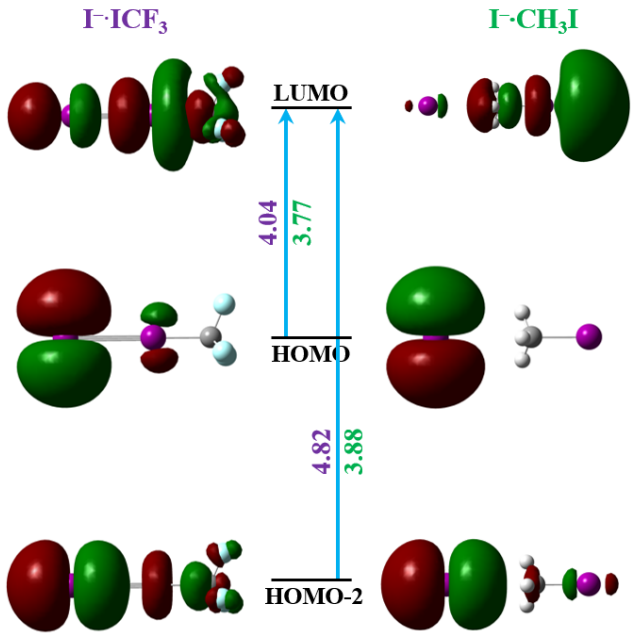

Figure 5: A comparison of the HOMO → LUMO and HOMO−2 → LUMO transitions of $I^-\cdots ICF_3$ and $I^-\cdots CH_3I$, respectively. Vertical excitation energies stated are in eV.

that of bare I^- is 3.06 eV.[81] The 0.36 eV increase in VDE upon clustering I^- to CH_3I has previously been attributed to the attractive interaction between the negative charge and the permanent dipole-moment of CH_3I (ignoring any interaction between neutral iodine and CH_3I).[28] This shift increases to 0.97 eV in $I^-\cdots ICF_3$ suggesting a significant degree of covalent bonding between I^- and ICF_3. This covalent bonding is apparent from the MOs shown in Figure 5 and the molecular structure in Figure 1 that indicate some $I_2^-\cdots CF_3$ character to the cluster. The calculated I–I distance in the complex is very similar to that of I_2^- (3.33 Å compared to 3.32 Å calculated at the same level of theory) and also show that the C–I bond in the complex (2.18 Å) is slightly elongated in comparison to CF_3I (2.14 Å). Hence, these observations suggest there is some I_2^- character and a weakening of the bonding interaction across the C–I bond. The covalent nature is also consistent with the increased spectral width of the PE peaks (~300 meV) compared to those observed in $I^-\cdots CH_3I$, which are on the order of 25 meV. The fact that the spectral shape for direct detachment is mostly Gaussian suggests that the final neutral state has a very different geometry to that of the anion.

Despite the apparent covalent character of the bonding in $I^-\cdots ICF_3$, it also retains much non-covalent character and has many similarities to $I^-\cdots CH_3I$. The degenerate lowest energy transitions are from the relatively non-binding p orbitals localised on I^-. While this transition carries a very small oscillator strength, its presence is consistent with the PE spectra at *hv* < 3.9 eV in Figure 2. Specifically, photodetachment from I^- can be seen by the narrow PE peak at eBE = 3.06 eV, which presumably comes about from excitation of $I^-\cdots ICF_3$ via the bound low-energy excited states that leads to dissociation of the cluster forming I^-. This atomic fragment can subsequently be photodetached in the presence of the laser field which remains present for ~ 5 ns (FWHM). The PE signal in this range was very small, consistent with the low oscillator strengths of the HOMO/HOMO−1 → LUMO transition and with the 2 sequential photon process.

For *hv* ≥ 3.80 eV, the total PE signal increases sharply. The total PE signal shown in Figure 4 has a peak at 3.97 eV. Concomitant to the increase in total PE yield is a change in the appearance of the PE spectrum: the detachment from I^- becomes a very minor channel while most signal appears at very low kinetic energy. This indirect detachment channel indicates that an intermediate excited state is accessed. Given the large increase in PE yield (Figure 4), we assign this to the calculated bright electronic transition (HOMO−2 → LUMO). As our calculations do not include spin-orbit coupling, the calculated transition energy is some way off. We do, of course, expect a spin-orbit component and this is clearly seen in Figure 2 as a second indirect channel opens up at *hv* ~ 4.9 eV (B in Figure 2).

At *hv* = 4.00 eV, there is a direct detachment peak from $I^-\cdots ICF_3$ and this peak remains present for *hv* ≥ 4.00 eV. We conclude that the bright state is very close to threshold. It is approximately 60 meV below the VDE. This also suggests that the total PE yield shown in Figure 4 is a convolution of the electron loss via the indirect channel and the direct detachment channel. Despite this complication, the second maximum observed at 4.07 eV does not correlate with this onset and appears to be an additional peak in the excitation cross section – *i.e.* a vibrational level of the excited state. The spacing of ~100 meV is very similar to that observed in the PE spectra (see Figure 3).

The observation of an excited state near threshold (for both spin-orbit channels) with vibrational structure is similar to observations in $I^-\cdots CH_3I$. In that case, vibrational progressions at 68 meV were observed in both the PE spectra and the photofragment action spectra monitoring I^- loss or electron loss. This vibrational progression was assigned to the ν_3 mode (based on the 66 meV frequency for the IR active ν_3 mode in CH_3I) and predominantly involves the C–I stretch. In their assessment of the $I^-\cdots CH_3I$ spectroscopy, Johnson and coworkers conclude that the vibrational structure in the PE spectra comes about from non-Franck-Condon (vibronic) effects.[28] The non-Franck-Condon behaviour was further supported by the fact that the vibrational activity seen in their PE spectra showed a dependence on the eKE of the outgoing electrons.[28]

Vibrational structure is also observed here in $I^-\cdots ICF_3$ and the vibrations appear more resolved at *hv* = 4.2 and 5.1 eV (see Figures 2 and 3), where the two spin-orbit thresholds open. In the case of CF_3I, the IR spectrum is dominated by the ν_1 and ν_2 mode (92 and 134 meV, respectively) of a_1 symmetry, which correspond to the symmetric CF_3 stretch and a C–I stretch (that also involves the CF_3 umbrella mode; this mode is similar to the ν_3 mode in CH_3I), respectively. Both these modes are close to the observed ~100 meV spacing in the PE spectrum (Figure 3) and the electron yield spectrum (Figure 4).

Cyr *et al*. probed the spectroscopy of $I^-\cdots CH_3I$ using electron yield as well as fragmentation action spectra with the two products being I^- and I_2^-. However, the main product is electron loss. In their PE spectra, no slow electrons were observed.[23] This may be because of the low collection efficiency at low eKE in their experiment. Here, we clearly show for $I^-\cdots ICF_3$ that the electrons are lost with a very low eKE. The mechanism ascribed by Johnson and co-workers for the dynamics is one in which the fragmentation can be viewed as an electron-molecule scattering process, leading to dissociation that is mediated by the σ* orbital along the C–I bond. This conclusion is consistent with the excited state calculated in Figure 5, where such a σ* character is clearly present. In the present case of $I^-\cdots ICF_3$, many analogies can be drawn. By inspection of the MO diagram in Figure 5, a similar σ* orbital is excited and an analogous vibrational progression involving the C–I stretch is seen in the PE spectra and photodetachment spectra of $I^-\cdots ICF_3$. Here, we have not been able to monitor atomic or molecular fragments directly and have only observed the electron loss channel. Nevertheless, it would appear that a similar overall mechanism can be ascribed here for $I^-\cdots ICF_3$. The fact that the indirect electrons appear at very low eKE, regardless of the photon energy may arise because the electrons are lost along the dissociative coordinate. It would clearly be of interest to perform fragment (probing I^- and I_2^-) action spectra, but these experiments are not possible in our current arrangement.

While the electronic structure of the S_N2 pre-reaction complexes appears little affected, clearly the stereochemistry has inverted. Therefore, $I^-\cdots ICF_3$ effectively serves as a probe for frontside attack entrance channel complex. As described in the introduction, recent crossed molecular beam experiments and simulations have shown that for the reactions $F^- + CH_3Y$, a change of Y = Cl to I led to an enhanced frontside attack, even though the long-range interactions is similar. Hence, it was suggested that a stronger interaction between F^- and I compared to F^- and Cl was responsible. In the present study, we have effectively trapped a frontside attack pre-reaction complex (with I^- as a reactant) and indeed, a significant covalent bonding character is observed. The binding energy can be roughly estimated from the increase in the VDE of the cluster relative to that of bare iodide. In the $I^-\cdots CH_3I$, this is 0.36 eV compared to 0.97 eV for $I^-\cdots ICF_3$. The former is a purely electron-dipole moment interaction and, assuming that the magnitude of the permanent dipole of CH_3I and CF_3I are similar, then the covalent contribution to the binding is approximately the difference in binding energy of $I^-\cdots CH_3I$ and $I^-\cdots ICF_3$ or ~0.6 eV. Although this is a very rough estimate, it does suggest that the covalent character is stronger than the overall repulsive charge-dipole moment interaction in $I^-\cdots ICH_3$ (0.36 eV). It would be of interest to study the $F^-\cdots CH_3I$ complex as a more direct comparison to the reaction dynamics studies, where a well depth of 0.97 eV was calculated for $F^-\cdots ICH_3$.[82–84] Overall, given the growing evidence of the existence and contributions of mechanisms other the traditional backside attack for S_N2 reactions,[10–12] the development of new experimental probes for complexes along such reaction coordinates should prove to be useful in determining energetics and structures of intermediates.

Conclusion

A photoelectron (PE) and photodetachment spectroscopic study of the $I^-\cdots ICF_3$ complex is presented, supported by DFT and TDDFT calculations. The binding in the cluster can be viewed as a combination between a non-covalent charge-dipole interaction and a covalent contribution along the I–I–C bond. The PE spectra show direct detachment channels, leaving the neutral in either spin-orbit states of the anion. The lowest vertical detachment energy is 4.03 eV and the adiabatic energy is approximately 3.8 eV. Near both thresholds, there is clear evidence of excitation to an excited state, which is corroborated by the PE yield spectrum around the first threshold. Electronic structure calculations show that this excited state can be assigned to a transition with charge-transfer character from the iodide to the ICF_3 moiety.

The spectroscopy is compared to the much-studied $I^-\cdots CH_3I$ cluster, which is the pre-reaction complex of the corresponding S_N2 reaction. The electronic structure of $I^-\cdots ICF_3$ shows many parallels, even though the geometric structure is very different because of the reversal of the dipole moment between CH_3I and CF_3I (*i.e*. the pre-reaction complex stereodynamics have been reversed). Specifically, both possess an excited state very close to threshold and show evidence of vibrational structure in the PE and photodetachment spectra. We assign the spectroscopy and excited state dynamics along parallel lines to that of $I^-\cdots CH_3I$: the excited state near threshold can be viewed as an electron scattering state that is strongly coupled to the σ* orbital on the I–C bond, leading to photoemission and dissociation (which was not measured here). We conclude that the overall electronic excited state structure is insensitive to the stereodynamics of the S_N2 pre-reaction complex.

Chemical dynamics simulations and crossed-beam imaging studies have recently shown that, for the $F^- + CH_3I$ reaction, the reaction is influenced by short-range attraction and often attacks as $F^- + ICH_3$,[9] implying that the covalent interaction of the pre-reaction complex is larger than the long-range electron-dipole interaction. The relatively strong covalent bonding observed between the two iodine atoms here may also be sufficient to overcome the repulsive electron-dipole moment interaction leading to an attractive well in the frontside attack of the $I^- + CH_3I$ S_N2 reaction. However, this well is weaker than the normal backside orientation as shown by the PE spectroscopy of Johnson and coworkers. In general, the replacement of H atoms with F atoms may serve as a useful general tool to invert the stereodynamics of S_N2 pre-reaction complexes, probe their interactions, and serve as a method for investigating non-traditional S_N2 reaction mechanisms.

Conflicts of interest

There are no conflicts to declare.

Acknowledgements

We thank Joshua P. Rogers for assistance with the experiment. This work was funded through an EPSRC Doctoral Training Grant.

References

1 K. P. C. Vollhardt and N. E. Schore, *Organic Chemistry: Structure and Function*, W. H. Freeman, New York, 5th edition., 2005.
2 C. G. Elles and F. F. Crim, Connecting Chemical Dynamics in Gases and Liquids, *Annu. Rev. Phys. Chem.*, 2006, **57**, 273–302.
3 J. M. Garver, Y. Fang, N. Eyet, S. M. Villano, V. M. Bierbaum and K. C. Westaway, A Direct Comparison of Reactivity and Mechanism in the Gas Phase and in Solution, *J. Am. Chem. Soc.*, 2010, **132**, 3808–3814.
4 A. J. Orr-Ewing, Perspective: Bimolecular chemical reaction dynamics in liquids, *J. Chem. Phys.*, 2014, **140**, 090901.
5 W. L. Hase, Simulations of Gas-Phase Chemical Reactions: Applications to S_N2 Nucleophilic Substitution, *Science*, 1994, **266**, 998–1002.
6 M. L. Chabinyc, S. L. Craig, C. K. Regan and J. I. Brauman, Gas-Phase Ionic Reactions: Dynamics and Mechanism of Nucleophilic Displacements, *Science*, 1998, **279**, 1882–1886.
7 J. K. Laerdahl and E. Uggerud, Gas phase nucleophilic substitution, *Int. J. Mass Spectrom.*, 2002, **214**, 277–314.
8 J. Mikosch, S. Trippel, C. Eichhorn, R. Otto, U. Lourderaj, J. X. Zhang, W. L. Hase, M. Weidemüller and R. Wester, Imaging nucleophilic substitution dynamics., *Science*, 2008, **319**, 183–186.
9 M. Stei, E. Carrascosa, M. A. Kainz, A. H. Kelkar, J. Meyer, I. Szabó, G. Czakó and R. Wester, Influence of the leaving group on the dynamics of a gas-phase S_N2 reaction, *Nat. Chem.*, 2016, **8**, 151–156.
10 J. Xie, R. Otto, J. Mikosch, J. Zhang, R. Wester and W. L. Hase, Identification of Atomic-Level Mechanisms for Gas-Phase $X^- + CH_3Y$ S_N2 Reactions by Combined Experiments and Simulations, *Acc. Chem. Res.*, 2014, **47**, 2960–2969.
11 I. Szabó and G. Czakó, Revealing a double-inversion mechanism for the F^-+CH_3Cl S_N2 reaction, *Nat. Commun.*, 2015, **6**, 5972.
12 J. Xie and W. L. Hase, Rethinking the S_N2 reaction, *Science*, 2016, **352**, 32–33.
13 C. E. H. Dessent and M. A. Johnson, Photoinitiation of Gas-Phase S_N2 Reactions through the Evans−Polanyi Excited State Surface, *J. Am. Chem. Soc.*, 1997, **119**, 5067–5068.
14 C. E. H. Dessent, J. Kim and M. A. Johnson, Photochemistry of Halide Ion−Molecule Clusters: Dipole-Bound Excited States and the Case for Asymmetric Solvation, *Acc. Chem. Res.*, 1998, **31**, 527–534.
15 R. Wester, A. E. Bragg, A. V. Davis and D. M. Neumark, Time-resolved study of the symmetric S_N2-reaction I^-+CH_3I, *J. Chem. Phys.*, 2003, **119**, 10032–10039.
16 J. Zhang, J. Mikosch, S. Trippel, R. Otto, M. Weidemüller, R. Wester and W. L. Hase, $F^- + CH_3I \rightarrow FCH_3 + I^-$ Reaction Dynamics. Nontraditional Atomistic Mechanisms and Formation of a Hydrogen-Bonded Complex, *J. Phys. Chem. Lett.*, 2010, **1**, 2747–2752.
17 J. Mikosch, J. Zhang, S. Trippel, C. Eichhorn, R. Otto, R. Sun, W. A. de Jong, M. Weidemüller, W. L. Hase and R. Wester, Indirect Dynamics in a Highly Exoergic Substitution Reaction, *J. Am. Chem. Soc.*, 2013, **135**, 4250–4259.
18 L. A. Angel and K. M. Ervin, Dynamics of the Gas-Phase Reactions of Fluoride Ions with Chloromethane, *J. Phys. Chem. A*, 2001, **105**, 4042–4051.
19 S. L. Vanorden, R. M. Pope and S. W. Buckner, Energy disposal in gas-phase nucleophilic displacement reactions, *Org. Mass Spectrom.*, 1991, **26**, 1003–1007.
20 T. Su, H. Wang and W. L. Hase, Trajectory Studies of S_N2 Nucleophilic Substitution. 7. $F^- + CH_3Cl \rightarrow FCH_3 + Cl^-$, *J. Phys. Chem. A*, 1998, **102**, 9819–9828.
21 Lide D. R., *Handbook of Chemistry and Physics*, CRC Press, Florida, 84th edn., 2003.
22 D. M. Cyr, G. A. Bishea, M. G. Scarton and M. A. Johnson, Observation of charge-transfer excited states in the $I^-\cdot CH_3I$, $I^-\cdot CH_3Br$, and $I^-\cdot CH_2Br_2$ S_N2 reaction intermediates using photofragmentation and photoelectron spectroscopies, *J. Chem. Phys.*, 1992, **97**, 5911–5914.
23 D. M. Cyr, C. G. Bailey, D. Serxner, M. G. Scarton and M. A. Johnson, The charge transfer excited state of the $I^-\cdot CH_3I$ S_N2 reaction intermediate: Photoinduced intracluster dissociative attachment, *J. Chem. Phys.*, 1994, **101**, 10507–10520.
24 S. S. Shaik and A. Pross, S_N2 reactivity of CH_3X derivatives. A valence bond approach, *J. Am. Chem. Soc.*, 1982, **104**, 2708–2719.
25 D. M. Cyr, M. G. Scarton and M. A. Johnson, Photoelectron spectroscopy of the gas-phase S_N2 reaction intermediates $I^-\cdot CH_3I$ and $I^-\cdot CD_3I$: Distortion of the CH_3I at the '"ion–dipole"' complex, *J. Chem. Phys.*, 1993, **99**, 4869–4872.
26 L. Deng, V. Branchadell and T. Ziegler, Potential Energy Surfaces of the Gas-Phase S_N2 Reactions $X^- + CH_3X = XCH_3 + X^-$ (X = F, Cl, Br, I): A Comparative Study by Density Functional Theory and ab Initio Methods, *J. Am. Chem. Soc.*, 1994, **116**, 10645–10656.
27 C. C. Arnold, D. M. Neumark, D. M. Cyr and M. A. Johnson, Negative Ion Zero Electron Kinetic Energy Spectroscopy of $I^-\cdot CH_3I$, *J. Phys. Chem.*, 1995, **99**, 1633–1636.
28 C. E. H. Dessent, C. G. Bailey and M. A. Johnson, On the vibrational fine structure in the near-threshold photofragmentation spectrum of the $I^-\cdot CH_3I$ complex: Spectroscopic observation of nonadiabatic effects in electron-molecule scattering, *J. Chem. Phys.*, 1996, **105**, 10416–10423.
29 R. Mabbs, E. Surber and A. Sanov, Photoelectron anisotropy and channel branching ratios in the detachment of solvated iodide cluster anions, *J. Chem. Phys.*, 2005, **122**, 054308.
30 M. Van Duzor, J. Wei, F. Mbaiwa and R. Mabbs, $I^-\cdot CH_3X$ (X=Cl,Br,I) photodetachment: The effect of electron-molecule interactions in cluster anion photodetachment spectra and angular distributions, *J. Chem. Phys.*, 2010, **133**, 144303.
31 S. Barnola, N. Posseme, S. Landis and M. Darnon, in *Plasma Etching Processes for CMOS Devices Realization*, Elsevier, 2017, pp. 59–94.
32 R. G. Poulsen, Plasma etching in integrated circuit manufacture—A review, *J. Vac. Sci. Technol.*, 1977, **14**, 266–274.
33 J. W. Coburn and H. F. Winters, Plasma etching—A discussion of mechanisms, *J. Vac. Sci. Technol.*, 1979, **16**, 391–403.
34 A. Sarangan, in *Fundamentals and Applications of Nanophotonics*, ed. J. W. Haus, Woodhead Publishing, 2016, pp. 149–184.
35 R. Reif, R. Chatterjee, S. Karecki and L. Pruette, in *Digest of Papers Microprocesses and Nanotechnology 2000. 2000 International Microprocesses and Nanotechnology Conference (IEEE Cat. No.00EX387)*, 2000, pp. 266-.

36 A. Misra, J. Sees, L. Hall, R. A. Levy, V. B. Zaitsev, K. Aryusook, C. Ravindranath, V. Sigal, S. Kesari and D. Rufin, Plasma etching of dielectric films using the non-global-warming gas CF_3I, *Mater. Lett.*, 1998, **34**, 415–419.

37 S. Samukawa, Y. Ichihashi, H. Ohtake, E. Soda and S. Saito, Environmentally harmonized CF_3I plasma for low-damage and highly selective low-k etching, *J. Appl. Phys.*, 2008, **103**, 053310.

38 E. Soda, S. Kondo, S. Saito, Y. Ichihashi, A. Sato, H. Ohtake and S. Samukawa, Low-damage low-k etching with an environmentally friendly CF_3I plasma, *J. Vac. Sci. Technol. A*, 2008, **26**, 875–880.

39 E. Soda, S. Kondo, S. Saito, K. Koyama, B. Jinnai and S. Samukawa, Mechanism of reducing line edge roughness in ArF photoresist by using CF_3I plasma, *J. Vac. Sci. Technol. B Microelectron. Nanometer Struct. Process. Meas. Phenom.*, 2009, **27**, 2117–2123.

40 Z. el Otell, V. Šamara, A. Zotovich, T. Hansen, J.-F. de Marneffe and M. R. Baklanov, Vacuum ultra-violet emission of CF_4 and CF_3I containing plasmas and Their effect on low-k materials, *J. Phys. Appl. Phys.*, 2015, **48**, 395202.

41 A. N. Goyette, Y. Wang and J. K. Olthoff, Comparison of the identities, fluxes, and energies of ions formed in high density fluorocarbon discharges, *AIP Conf. Proc.*, 2001, **550**, 238–242.

42 S. Marienfeld, I. I. Fabrikant, M. Braun, M.-W. Ruf and H. Hotop, High resolution low-energy electron attachment to CF_3I, *J. Phys. B At. Mol. Opt. Phys.*, 2006, **39**, 105.

43 U. Even, J. Jortner, D. Noy, N. Lavie and C. Cossart-Magos, Cooling of large molecules below 1 K and He clusters formation, *J. Chem. Phys.*, 2000, **112**, 8068–8071.

44 B. Bandyopadhyay, T. Stein, Y. Fang, O. Kostko, A. White, M. Head-Gordon and M. Ahmed, Probing Ionic Complexes of Ethylene and Acetylene with Vacuum-Ultraviolet Radiation, *J. Phys. Chem. A*, 2016, **120**, 5053–5064.

45 W. C. Wiley and I. H. McLaren, Time-of-Flight Mass Spectrometer with Improved Resolution, *Rev. Sci. Instrum.*, 1955, **26**, 1150–1157.

46 A. T. J. B. Eppink and D. H. Parker, Velocity map imaging of ions and electrons using electrostatic lenses: Application in photoelectron and photofragment ion imaging of molecular oxygen, *Rev. Sci. Instrum.*, 1997, **68**, 3477–3484.

47 D. A. Horke, G. M. Roberts, J. Lecointre and J. R. R. Verlet, Velocity-map imaging at low extraction fields, *Rev. Sci. Instrum.*, 2012, **83**, 063101.

48 G. M. Roberts, J. L. Nixon, J. Lecointre, E. Wrede and J. R. R. Verlet, Toward real-time charged-particle image reconstruction using polar onion-peeling, *Rev. Sci. Instrum.*, 2009, **80**, 053104.

49 W. Kohn and L. J. Sham, Self-Consistent Equations Including Exchange and Correlation Effects, *Phys. Rev.*, 1965, **140**, A1133–A1138.

50 E. Runge and E. K. U. Gross, Density-Functional Theory for Time-Dependent Systems, *Phys. Rev. Lett.*, 1984, **52**, 997–1000.

51 J. M. Galbraith and H. F. Schaefer, Concerning the applicability of density functional methods to atomic and molecular negative ions, *J. Chem. Phys.*, 1996, **105**, 862–864.

52 N. Rösch and S. B. Trickey, Comment on "Concerning the applicability of density functional methods to atomic and molecular negative ions" [J. Chem. Phys. 105, 862 (1996)], *J. Chem. Phys.*, 1997, **106**, 8940–8941.

53 S. Hirata, M. Head-Gordon, J. Szczepanski and M. Vala, Time-Dependent Density Functional Study of the Electronic Excited States of Polycyclic Aromatic Hydrocarbon Radical Ions, *J. Phys. Chem. A*, 2003, **107**, 4940–4951.

54 G. Malloci, G. Mulas, G. Cappellini and C. Joblin, Time-dependent density functional study of the electronic spectra of oligoacenes in the charge states -1, 0, +1 , and +2, *Chem. Phys.*, 2007, **340**, 43–58.

55 H.-Y. Cheng and Y.-S. Huang, Temporary anion states of *p*-benzoquinone: shape and core-excited resonances, *Phys. Chem. Chem. Phys. PCCP*, 2014, **16**, 26306–26313.

56 M. F. Falcetta, L. A. DiFalco, D. S. Ackerman, J. C. Barlow and K. D. Jordan, Assessment of Various Electronic Structure Methods for Characterizing Temporary Anion States: Application to the Ground State Anions of N_2, C_2H_2, C_2H_4, and C_6H_6, *J. Phys. Chem. A*, 2014, **118**, 7489–7497.

57 T. Yanai, D. P. Tew and N. C. Handy, A new hybrid exchange–correlation functional using the Coulomb-attenuating method (CAM-B3LYP), *Chem. Phys. Lett.*, 2004, **393**, 51–57.

58 M. J. G. Peach, A. M. Teale, T. Helgaker and D. J. Tozer, Fractional Electron Loss in Approximate DFT and Hartree–Fock Theory, *J. Chem. Theory Comput.*, 2015, **11**, 5262–5268.

59 M. J. G. Peach, P. Benfield, T. Helgaker and D. J. Tozer, Excitation energies in density functional theory: an evaluation and a diagnostic test, *J. Chem. Phys.*, 2008, **128**, 044118.

60 A. U. Hazi and H. S. Taylor, Stabilization Method of Calculating Resonance Energies: Model Problem, *Phys. Rev. A*, 1970, **1**, 1109–1120.

61 M. J. Frisch, J. A. Pople and J. S. Binkley, Self-consistent molecular orbital methods 25. Supplementary functions for Gaussian basis sets, *J. Chem. Phys.*, 1984, **80**, 3265–3269.

62 R. Krishnan, J. S. Binkley, R. Seeger and J. A. Pople, Self-consistent molecular orbital methods. XX. A basis set for correlated wave functions, *J. Chem. Phys.*, 1980, **72**, 650–654.

63 A. D. McLean and G. S. Chandler, Contracted Gaussian basis sets for molecular calculations. I. Second row atoms, Z=11–18, *J. Chem. Phys.*, 1980, **72**, 5639–5648.

64 T. H. Dunning and P. J. Hay, in *Methods of Electronic Structure Theory*, Springer, Boston, MA, 1977, pp. 1–27.

65 P. J. Hay and W. R. Wadt, Ab initio effective core potentials for molecular calculations. Potentials for K to Au including the outermost core orbitals, *J. Chem. Phys.*, 1985, **82**, 299–310.

66 W. R. Wadt and P. J. Hay, Ab initio effective core potentials for molecular calculations. Potentials for main group elements Na to Bi, *J. Chem. Phys.*, 1985, **82**, 284–298.

67 M. Frisch, G. Trucks, H. Schlegel, G. Scuseria, M. Robb, J. Cheeseman, G. Scalmani, V. Barone, B. Mennucci, G. Petersson, H. Nakatsuji, M. Caricato, X. Li, H. Hratchian, A. Izmaylov, J. Bloino, G. Zheng, J. Sonnenberg, M. Hada, M. Ehara, K. Toyota, R. Fukuda, J. Hasegawa, M. Ishida, T. Nakajima, Y. Honda, O. Kitao, H. Nakai, T. Vreven, J. Montgomery, J. Peralta, F. Ogliaro, M. Bearpark, J. Heyd, E. Brothers, K. Kudin, V. Staroverov, R. Kobayashi, J. Normand, K. Raghavachari, A. Rendell, J. Burant, S. Iyengar, J. Tomasi, M. Cossi, N. Rega, J. Millam, M. Klene, J. Knox, J. Cross, V. Bakken, C. Adamo, J. Jaramillo, R. Gomperts, R. Stratmann, O. Yazyev, A. Austin, R. Cammi, C. Pomelli, J. Ochterski, R. Martin, K. Morokuma, V. Zakrzewski, G. Voth, P. Salvador, J. Dannenberg, S. Dapprich, A. Daniels, Farkas, J. Foresman, J. Ortiz, J. Cioslowski and D. Fox, Gaussian 09, *Gaussian 09 Gaussian Inc Wallingford CT*.

68 S. Grimme, J. Antony, S. Ehrlich and H. Krieg, A consistent and accurate ab initio parametrization of density functional dispersion correction (DFT-D) for the 94 elements H-Pu, *J. Chem. Phys.*, 2010, **132**, 154104.

69 M. J. Frisch, M. Head-Gordon and J. A. Pople, A direct MP2 gradient method, *Chem. Phys. Lett.*, 1990, **166**, 275–280.

70 J. Gadhi, G. Wlodarczak, J. Legrand and J. Demaison, The dipole moments of methyl bromide and methyl iodide, *Chem. Phys. Lett.*, 1989, **156**, 401–404.

71 A. P. Cox, G. Duxbury, J. A. Hardy and Y. Kawashima, Microwave spectra of CF_3Br and CF_3I. Structures and dipole moments, *J. Chem. Soc. Faraday Trans. 2 Mol. Chem. Phys.*, 1980, **76**, 339–350.

72 C. S. Anstöter, J. N. Bull and J. R. R. Verlet, Ultrafast dynamics of temporary anions probed through the prism of photodetachment, *Int. Rev. Phys. Chem.*, 2016, **35**, 509–538.

73 C. W. West, J. N. Bull, E. Antonkov and J. R. R. Verlet, Anion Resonances of para-Benzoquinone Probed by Frequency-Resolved Photoelectron Imaging, *J. Phys. Chem. A*, 2014, **118**, 11346–11354.

74 J. N. Bull, C. W. West and J. R. R. Verlet, On the formation of anions: frequency-, angle-, and time-resolved photoelectron imaging of the menadione radical anion, *Chem. Sci.*, 2015, **6**, 1578–1589.

75 C. W. West, J. N. Bull, A. S. Hudson, S. L. Cobb and J. R. R. Verlet, Excited State Dynamics of the Isolated Green Fluorescent Protein Chromophore Anion Following UV Excitation, *J. Phys. Chem. B*, 2015, **119**, 3982–3987.

76 C. S. Anstöter, C. R. Dean and J. R. R. Verlet, Chromophores of chromophores: a bottom-up Hückel picture of the excited states of photoactive proteins, *Phys. Chem. Chem. Phys.*, 2017, **19**, 29772–29779.

77 J. N. Bull and J. R. R. Verlet, Dynamics of π*-resonances in anionic clusters of para-toluquinone, *Phys. Chem. Chem. Phys.*, 2017, **19**, 26589–26595.

78 J. P. Rogers, C. S. Anstöter and J. R. R. Verlet, Ultrafast dynamics of low-energy electron attachment via a non-valence correlation-bound state, *Nat. Chem.*, 2018, **10**, 341–346.

79 J. P. Rogers, C. S. Anstöter and J. R. R. Verlet, Evidence of Electron Capture of an Outgoing Photoelectron Wave by a Nonvalence State in $(C_6F_6)_n^-$, *J. Phys. Chem. Lett.*, 2018, **9**, 2504–2509.

80 D. Serxner, C. E. H. Dessent and M. A. Johnson, Precursor of the Iaq− charge-transfer-to-solvent (CTTS) band in $I^-\cdot(H_2O)_n$ clusters, *J. Chem. Phys.*, 1996, **105**, 7231–7234.

81 D. Hanstorp and M. Gustafsson, Determination of the electron affinity of iodine, *J. Phys. B At. Mol. Opt. Phys.*, 1992, **25**, 1773.

82 P. G. Wenthold, D. A. Hrovat, W. T. Borden and W. C. Lineberger, Transition-State Spectroscopy of Cyclooctatetraene, *Science*, 1996, **272**, 1456–1459.

83 D. M. Neumark, Transition State Spectroscopy of Bimolecular Chemical Reactions, *Annu. Rev. Phys. Chem.*, 1992, **43**, 153–176.

84 J. B. Kim, M. L. Weichman, T. F. Sjolander, D. M. Neumark, J. Kłos, M. H. Alexander and D. E. Manolopoulos, Spectroscopic observation of resonances in the F + H_2 reaction, *Science*, 2015, **349**, 510–513.